



Battery-on-Separator: A platform technology for arbitrary-shaped lithium ion batteries for high energy density storage

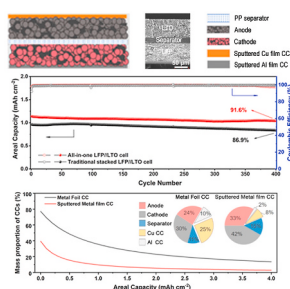
Min Wang^{a,b}, Wentao Yao^a, Peichao Zou^{a,c}, Shengyu Hu^a, Haojie Zhu^{a,b}, Kangwei Liu^{a,b}, Cheng Yang^{a,*}

^a Institute of Materials Research, Tsinghua Shenzhen International Graduate School, Tsinghua University, Shenzhen, 518055, PR China

^b School of Materials Science and Engineering, Tsinghua University, Beijing, 100084, PR China

^c Department of Physics and Astronomy, University of California, Irvine, CA, 92697, USA

GRAPHICAL ABSTRACT



ARTICLE INFO

Keywords:

Arbitrary-shaped
Current collectors
Magnetron sputtering
High energy density
Lithium-ion batteries

ABSTRACT

Arbitrary-shaped batteries with high energy densities are strongly desired for weight- and power-sensitive applications to meet various layout and function demands. Conventional battery electrode fabrication protocol requires a relatively thick metal foil (9–15 μm) to provide sufficient mechanical strength for slurry coating, leading to high occupancy of inactive components. Besides, conventional battery assembly methods result in limited battery layouts, which is difficult for well-fitting complex-shaped electronics. To overcome these limitations, developing novel battery fabrication technologies is critically urgent and important. Herein, we report a scalable method to fabricate arbitrary-shaped lithium-ion batteries with ultra-thin current collectors. Built on a commercial polypropylene separator, an all-in-one structured lithium ion battery is fabricated by integrating active material layers and ultra-thin metal film current collectors (optimally 2- μm -thick) through stencil printing and magnetron sputtering methods. By reducing the thickness of current collectors down to 2 μm , the energy density of a $\text{LiFePO}_4/\text{Li}_4\text{Ti}_5\text{O}_{12}$ full cell can be increased by 16%–64% based on the designed areal capacities between 1 mAh cm^{-2} to 3 mAh cm^{-2} . Such battery fabrication method can effectively realize the shape diversity of electrodes, thereupon enabling the seamless integration of arbitrary-shaped batteries into versatile portable electronics to improve their space utilization.

* Corresponding author.

E-mail address: yang.cheng@sz.tsinghua.edu.cn (C. Yang).

<https://doi.org/10.1016/j.jpowsour.2021.229527>

Received 1 January 2021; Accepted 16 January 2021

Available online 1 February 2021

0378-7753/© 2021 Published by Elsevier B.V.

1. Introduction

The rapid development of smart electronic devices technologies such as smartphones, smartwatches, and small drones arouse imminent demands for high energy density lithium-ion batteries (LIBs) and shape tolerable design [1–3]. Traditional battery assembly processes including electrode wet coating, tailoring, cell stacking, etc., lead to the shape (cylindrical, prismatic, and pouch) limitation of batteries, which limited their applications. Besides, these conventional processes also limit the energy density improvement of batteries. The gravimetric and volumetric energy densities of a LIB not only depend significantly on the capacity of active materials, but also include the weight/volume influence of inactive components in the battery, such as the packaging materials, current collectors (CCs), and tabs. These indispensable inactive components have no contribution to the overall capacity, yet occupying a large weight/volume proportion of the cell pack. For instance, conventional LIBs fabrication technique requires casting electrode slurry onto metal foil CCs, typically using 9- μm -thick Cu foils for the anode and 15- μm -thick Al foils for the cathode. The Cu and Al foils account for 15% and 50% of the total mass of the cathode and anode, respectively [4]. The effective specific capacity of anodes can be improved by 23%–49%, if the thickness of the Cu CCs is reduced to 5 μm or even to 2 μm , in which the graphite anode with a mass loading of 10 mg cm^{-2} and 10 wt % binder and carbon additives was used as the baseline [5,6]. By simply reducing the thickness of the CCs without changing the active materials, the energy density of most LIBs systems can be improved. However, it's still challenging to produce free-standing metal foils with thickness less than 5 μm for battery manufacturing [7], largely due to the wrinkling and fracture issues of thin metal foils, which are also too difficult to handle during the conventional slit coating process [8]. With the surging demand for higher energy density per unit cell, it's critically important to explore novel battery fabrication technology and related key materials to reduce the mass proportion of inactive CCs as much as possible. The relevant technological breakthrough of ultrathin CCs would make a profound impact on future energy storage technologies [9,10].

Physical vapor deposition (PVD) has been an effective method to fabricate ultrathin and dense metal film with strong adhesion to the substrates, which could be a potential choice to realize ultrathin CCs. Using the PVD method such as magnetron sputtering or evaporation to deposit a metal film on a polymeric substrate have been studied as potential ultrathin CCs materials in lithium ion batteries [11,12]. These PVD process generally involves a non-conductive substrate to support the deposited film. However, the single-side conductive compound CC could introduce additional inactive components when used in multi-layer laminated batteries. For example, Kang et al. deposited thin metal CCs on the inner surface of an Al-plastic pouch to improve the energy density of thin-film LIBs [11]. Unfortunately, this method could increase the proportion of inactive Al-plastic film when used in multi-layer battery and thus was only demonstrated viable for single-layer battery fabrication. Targeted at reducing inactive components and reach a higher integration level, the all-in-one architecture design is further proposed in which all components are layer-by-layer prepared and integrated into one substrate [13–15]. In the all-in-one energy storage devices, the lightweight separators are often adopted as the only substrates instead of CCs to load the other components [16–18], and thus can reduce the thickness and proportion of CCs and other inactive substrates. Yet this technology is mainly applied to the research of solid-state thin-film batteries [19] and micro-batteries [20] in which the active materials, ultrathin CCs are deposited on one substrate to construct the monolithic structured by PVD. The thicknesses of the deposited electrode are limited by a few micrometers because higher thickness will lead to crack formation and film failure caused by mechanical stress. Thus these all-in-one batteries can only output limited energy (0.1–1 $\text{J cm}^{-2} \mu\text{m}^{-1}$) and are usually used for low-energy applications [21]. Yao et al. constructed a high-energy all-in-one Li-S battery via wet coating S cathode and depositing Li anode on the two

sides of a commercial polypropylene (PP) separator [22]. However, this process also needs the additional free-standing Cu and Al foil as the CCs. To the best of our knowledge, rare reports are employing ultrathin CCs construction into the monolithically integrated structure to improve the energy density of high-capacity ($>1 \text{ mAh cm}^{-2}$) LIBs.

Herein, we designed a kind of new monolithic integrated LIBs with ultrathin CCs based on stencil printing and magnetron sputtering methods using PP separator as the initial substrate to achieve arbitrary-shaped lithium ion batteries with high energy densities. Experimental results showed that the method of directly sputtering metal film on the surface of the active material layer can produce compact and ultrathin metal CCs with high electronic conductivities. The ultrathin CCs can also be tightly connected with the active material layer. We demonstrate that when the thickness of the sputtered CCs is 2 μm , the monolithic LIB can maintain excellent electrochemical performance. In a $\text{LiFePO}_4/\text{Li}_4\text{Ti}_5\text{O}_{12}$ ($\sim 1 \text{ mAh cm}^{-2}$) full cell system, the mass proportion of the CCs in the battery was reduced by 71%, and the full cell gravimetric energy density can be increased by 40% compared with that of a full cell built on conventional metal foil CCs. Furthermore, this sputtering technique is also compatible with various classical lithium-ion battery anodes and cathodes, such as graphite, LiCoO_2 (LCO) and $\text{LiNi}_{0.8}\text{Co}_{0.15}\text{Al}_{0.05}\text{O}_2$ (NCA). By leveraging this unique technology, we demonstrate an alien-shaped battery and it can be fitted to drive a bird-shaped flapping-wing aircraft without damaging its aerodynamic feature. This work demonstrates an effective strategy to fabricate printable monolithic integrated LIBs with ultra-thin CCs, which not only delivers improved energy density for the all-in-one cells but also provides feasibilities in making arbitrary-shaped energy devices.

2. Experimental section

2.1. Preparation of electrodes

All the active materials adopted for cathodes and anodes preparation are commercial, including LFP, LCO, Graphite, NCA, and LTO. For the preparation of cathode slurry, LFP (or LCO), Super P (TIMCAL Co.), and polyvinylidene fluoride (PVDF, Solvay Co.) were dispersed at a weight ratio of 8:1:1 in an appropriate amount of N-methyl-2-pyrrolidone (NMP) and stirred in a planetary mixer (Hasai 300, HASAI Co.). Similarly, the LTO, Super P, and PVDF (8:1:1) were used for the anode slurry preparation.

For the fabrication of all-in-one structure cells, the cathode active material layer was prepared by coating the cathode slurry on one side of the PP separator (Celgard 2500) via stencil printing technique (stainless steel-based stencils with different sizes and shapes of hollow patterns were used), followed by vacuum drying at 60 $^{\circ}\text{C}$ for overnight. The anode active layer material layer was obtained on the other side of the PP separator by the same method. For the assembly of full cells, the diameters of paired cathode and anode were 14 mm and 12 mm, respectively, and the N/P ratio is controlled at 0.9. For example, the active mass loadings of cathode and anode for 1 mAh cm^{-2} LFP//LTO cell were around 7.5 mg cm^{-2} (1.1 mAh cm^{-2}) and 6.1 mg cm^{-2} (1 mAh cm^{-2}), respectively. For half-cells (1 mAh cm^{-2} type), the mass loadings of LFP, LCO, and LTO were around 7.0 mg cm^{-2} , 7.1 mg cm^{-2} , and 6.1 mg cm^{-2} , respectively, and the diameter of all coated electrodes is 12 mm. Thereafter, the coated sample was roll-pressed by a small roller. After the calendar process, a thin Al (Cu) layer was coated on the surface of cathode (anode) active material layer as CCs by magnetron sputtering in Ar-protected atmosphere (with an air pressure of 0.3 Pa and operation power of 1.6 kW for the deposition rate of about 30 nm min^{-1} for Al and 40 nm min^{-1} for Cu); in this process, the exposed separator areas were protected by polyimide (PI) mask. Finally, the PP-based electrodes were punched into discs with a diameter of 20 mm for coin cell assembly or other shapes for pouch cell assembly.

Regarding the preparation of control electrodes based on metal foil CCs, the same electrode slurries were used as those for coated electrodes.

The difference is that the slurry was blade coated on the Al foil (12 μm in thickness) and Cu foil (9 μm in thickness) to obtain the cathodes and anodes, respectively. After drying and rolling, the electrodes were punched into discs with a diameter of 12 mm (or 14 mm) for coin cell testing.

2.2. Battery assembly

In terms of the assembly of coin-type half cells, the active material layer was only coated on one side of the PP separator as a working electrode and lithium foil (15.6 mm in diameter, and 450 μm in thickness) was used as the counter/reference electrode. All coin-type (CR2032) cells and pouch cells were assembled in an argon-filled glove box. 1 M LiPF_6 in ethylene carbonate/ethyl methyl carbonate/dimethyl carbonate (EC/EMC/DMC, 1:1:1 in volume) was utilized as the electrolyte for LFP//LTO system, while the electrolyte consisting of 1 M LiPF_6 in FEC/EMC/DMC (1:1:1 in volume) was used for LCO//LTO system.

During the assembly of arbitrary-shaped pouch cells, after cutting the AIO electrodes into desired shapes, the Al and Ni tabs were attached to the cathode and anode CCs by conductive carbon slurry, respectively. The carbon slurry was composed of graphene, Super P, and PVDF with a mass ratio of 6:1:1, and the NMP was used as the solvent. The sheet resistance of the conductive carbon films is $8 \Omega \text{sq}^{-1}$ (20 μm in thickness). Afterward, the AIO electrode was put into an aluminum-plastic film bag, and encapsulated by a heat sealer after injecting 0.6 mL electrolyte.

2.3. Characterizations and electrochemical measurements

The morphologies of electrodes were characterized by field-emission scanning electron microscopy (SEM, HITACHI S4800). X-ray diffraction (XRD) patterns were collected to analyze the structure of the materials via the X-ray diffractometer (D8 Advance). The sheet resistances of the metal foils and sputtered metal films were tested by the four-probe method via a resistance analyzer instrument (MCP-T610, LA RESTA-GP). The vertical resistance of electrodes was tested by controlled voltage double probe resistance method via a dual-probe resistance test instrument (TT-ACCF-G1, ACC Film tech., China), during which free-standing electrode sheets were prepared by slit coating slurry on the release films, and the metal film CCs was sputtered on the free-standing electrodes to prepare the ultrathin film CCs based single electrode sheets. Electrochemical impedance spectroscopy (EIS, 100 kHz-10 mHz at a potential amplitude of 10 mV) and cyclic voltammetry (CV) measurements were performed on an electrochemical station (VMP3, Bio-Logic). Galvanostatic charge-discharge (GCD) cycles, rate, and cycling performance of cells were conducted by a Land battery test system (Wuhan Land Electronic Co., China) at room temperature.

3. Results and discussion

The schematic fabrication process of all-in-one LIBs based on ultrathin CCs is illustrated in Fig. 1. Primarily, the cathode and anode slurries are stencil-printed on two sides of a commercial PP separator in sequence. By designing different stencil mask patterns, various geometric shapes of electrodes can be obtained as displayed in Fig. 1. Although the commercial polymer LIB separator already has high mechanical strength and stable electrochemical characterization, this separator based assembly process requires a higher quality separator for AIO cell. Firstly, the separator should have few defects, smaller pore size than electrode particles and high mechanical strength to support the printed electrode slurry and avoid short-circuit during electrode rolling. Secondly, the separator needs to be chemically stable towards sensitive compositions such as solvent and binder in electrode slurry. Thirdly, the thermal stability of separator is of importance to withstand the heat generation in the sputtering process. The PP separators are robust with

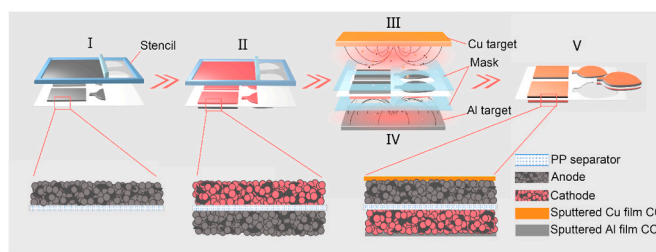


Fig. 1. Schematic illustration for the preparation of the all-in-one cell: (I) stencil-printing of anode slurry on the one side of a commercial PP separator; (II) stencil-printing cathode slurry on the other side of the PP separator; (III, IV) magnetron sputtering the ultra-thin (III) Cu film on the anode layer and (IV) Al film on the cathode layer; (V) cutting off the all-in-one electrodes into desired size and shapes, and filled with liquid electrolytes.

excellent mechanical properties [23], making them ideal candidates as the initial substrates. Besides, the ellipsoidal pore size of PP separators (0.21 μm in length, and 0.05 μm in width) is smaller than the electrode material particles, which can effectively avoid short circuit between cathode and anode (Figs. S1 and S2). Subsequently, the as-printed electrode undergoes a calendar process, to enhance the partial contact and reduce the surface roughness of active material layers (Fig. S3) which offers an even surface for the following deposition of metal CCs. Then, Al and Cu film CCs were coated on the cathode and anode active material layer respectively by magnetron sputtering, affording the all-in-one structure cell (AIO cell). High electronic conductivity is one prerequisite for CCs applied in LIBs. By controlling the thickness of the sputtered metal films, CCs with different conductivities can be obtained as shown in Fig. S4. When the thicknesses of both Al and Cu films decrease to less than 2 μm , their surface resistances increase abruptly. In contrast, as the metal film thickness is increased to 2 μm or higher, the surface resistances tend to be maintained at $0.2 \Omega \text{sq}^{-1}$. Meanwhile, a homogeneous and compact film can be obtained when the thickness is 2 μm or higher (Figs. S5 and S6). Thus, the optimum thicknesses of both Cu and Al metal film CCs are determined to be 2 μm . According to the XRD results of LFP/Sputtered Al CC and LTO/Sputtered Cu CC electrodes (Fig. S7), apart from the Cu (JCPDS card NO.03-065-9743) and Al (JCPDS card NO.96-230-0251) patterns, the XRD patterns of LTO and LFP electrodes fit well with standard JCPDS card NO.96-100-1099 and NO.96.210-0917, respectively. These results show that the crystalline phase of active materials did not change after metal film sputtering.

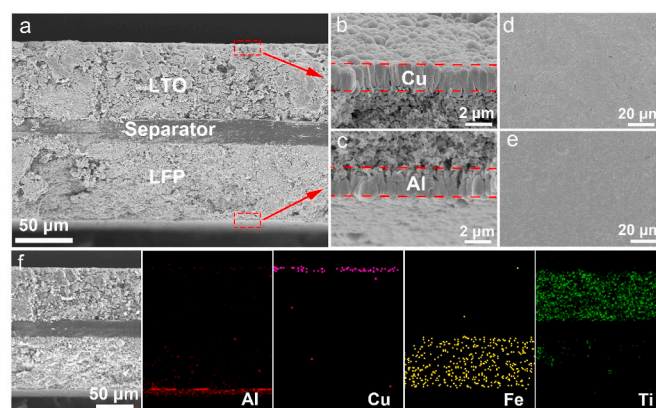


Fig. 2. Morphological and compositional characterizations of the all-in-one LFP//LTO cell. (a) Cross-sectional SEM images of the cell. (b, c) Cross-sectional SEM images of (b) Cu film and (c) Al film from the selected area in (a), marked by red dashed lines. (d, e) Over-view SEM images of (d) Cu film and (e) Al film. (f) The corresponding EDS mappings of the cell. (For interpretation of the references to colour in this figure legend, the reader is referred to the Web version of this article.)

According to the cross-sectional SEM images and corresponding elemental mapping images of the AIO cell (Fig. 2a and f), it can be seen that the sputtered Al and Cu film CCs were rather thin compared with the active material layers. The compact surface of 2- μm -metal film CCs (Fig. 2c and e) is conductive with high electrochemical stability. Additionally, the sputtered metal films were vertically aligned on the active material layer and displayed a columnar structure [24], which is beneficial to the improvement of overall out-of-plane electronic conductivity [25]. Moreover, since magnetron sputtering is a high-energy atomic deposition process, the relatively large surface roughness of substrates (*i.e.*, LTO and LFP layers) makes it possible to form a tight mechanical occlusal interface between substrates and the sputtered metal film CCs. As revealed in Fig. 2b and c, the sputtered metal film CCs are in closer contact with the active material layers without any visible gap compared with metal foil CCs (Figs. S8 and S9). In the all-in-one structure, the contact resistance between the active material layers and CCs could be minimized due to the increased interface contact area. The overall out-of-plane resistances of single electrodes based on different CCs were measured via a controlled voltage double probe resistance method in which every single electrode consists of one active material layer and one CC layer (see details in the experimental section). Although the sheet resistance of the ultra-thin CCs is much larger than that of the metal foils, the film resistance of metal film CCs based electrodes is comparable to or even slightly lower than that of traditional metal foil based electrodes (Fig. S10). This result indicates that good electronic conductivity of the electrode can be maintained even when the thickness of the CC was reduced.

Half-cells based on LTO and LFP electrodes with both ultrathin metal films and commercial metal foils were assembled for electrochemical testing. Electrochemical impedance spectroscopy (EIS) measurement of the LFP electrode was conducted in a half-cell configuration (LFP//Li),

and the collected impedance spectra (Fig. 3a, b) were fitted by an equivalent circuit model (Fig. S11) to calculate the ohmic internal resistance R_s . The value of the R_s reflects the internal resistances of all the components in the battery, including the resistance of CCs, separator, active materials, electrolyte, and contact resistance between these layers. Presuming that the mass loadings of active materials, separator, and electrolyte dosage are consistent, the values of R_s shall reflect the effect of the CCs on the internal resistance of the battery. Before cycling, the R_s of pristine LFP/Sputtered Al film electrode (3.4 Ω) is comparable with that of the LFP/Al foil electrode (3.3 Ω). After 2, 50, and 100 cycles at 1C, the R_s of LFP/Sputtered Al film electrode only changed slightly, suggesting high structural stability of the ultrathin sputtered metal CCs during cycling (the simulation results are listed in Table S1). Similar results can also be obtained from the EIS data of the LTO/Sputtered Cu film electrode and LTO/Cu foil CC electrode (Fig. S12 and Table S2). Here, the similar resistance of these two kinds of batteries is due to the equal longitudinal electrical conductivity of the ultrathin CCs and metal foil CCs based electrodes (Fig. S10). Furthermore, the LFP/Sputtered Al film electrode delivered a reversible specific capacity of about 152 mAh g^{-1} reversible specific capacity with first cycle coulombic efficiency of about 99%, which are very close to those of LFP/Al foil electrode (Fig. 3c). Likewise, the LTO/Sputtered Cu film and the LTO/Cu foil electrodes also exhibited a similar capacity and coulombic efficiency at the first cycle (Fig. 3d). Moreover, even at higher rates, all these electrodes can still maintain high specific capacities (Fig. 3e). After 100 charge and discharge cycles, the capacity retention of LFP/Sputtered Al film and LTO/Sputtered Cu film electrodes were 96% and 95%, respectively (Fig. 3f), indicating excellent long-term cycling stability of the ultra-thin metal film CCs.

To further explore the merits of the sputtered metal film CCs for lithium-ion battery applications, all-in-one LFP//LTO full cells were assembled. In the LFP//LTO full cell system, when the areal capacity reached 1.1 mAh cm^{-2} , the first cycle coulombic efficiency of the AIO full cell was 84% (Fig. 4a). Impressively, the AIO LFP//LTO full cell exhibits a smaller charge transfer resistance R_{ct} of 13.5 Ω than the traditional stacked full cell, despite their R_s is very similar (Fig. 4b). That indicates that the AIO full cell presents faster electrochemical kinetics than the traditional stacked full cell, owing to the seamless connection between adjacent components (Fig. 2a) that enable a continuous electron-/ion transfer pathway [22]. Meanwhile, the AIO LFP//LTO full cell

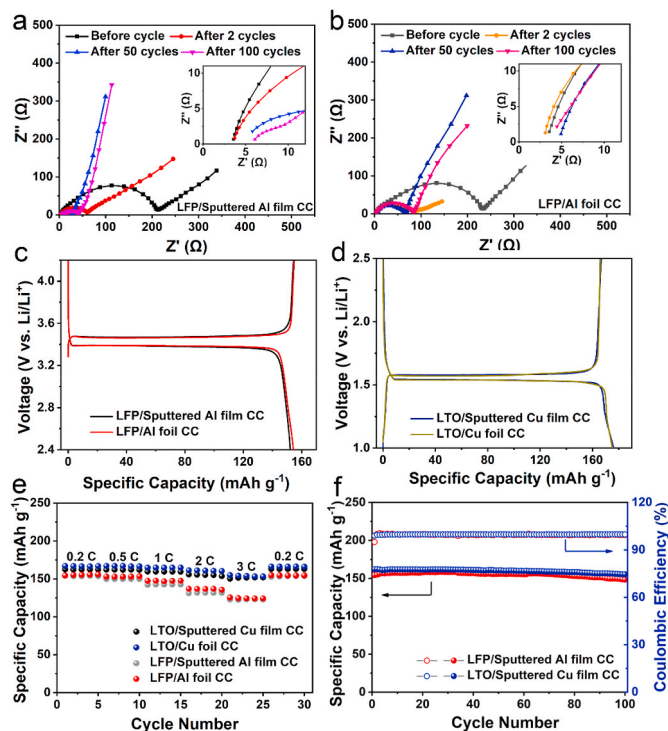


Fig. 3. Electrochemical performance evaluation of LFP and LTO electrodes with metal foil or sputtered metal film as CCs. (a, b) EIS spectra of LFP electrodes with (a) sputtered Al film CCs and (b) Al foil CCs. (c, d) Galvanostatic charge-discharge (GCD) profiles of (c) LFP and (d) LTO electrodes at the first cycle of 0.1C with different CCs. (e) Rate performance of LFP and LTO electrodes with different CCs. (f) Cycling performance of LFP and LTO electrodes with sputtered metal film CCs at 0.5C.

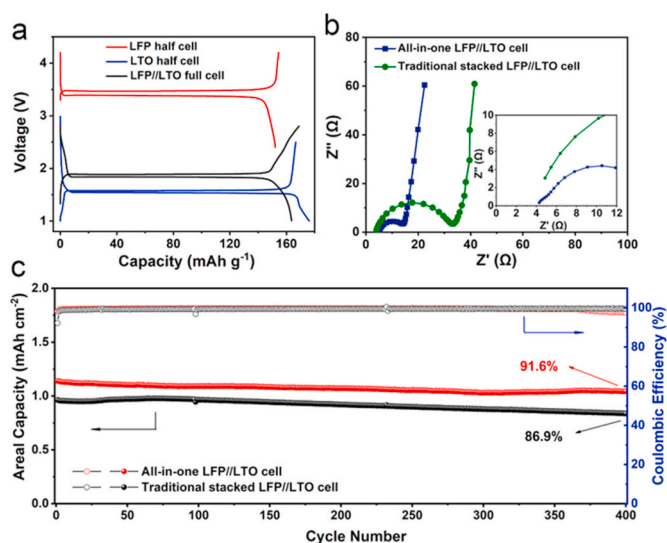


Fig. 4. Electrochemical performance evaluation of LFP//LTO full-cells with metal foil and sputtered metal film as CCs. (a) The first cycle GCD profiles of LFP half-cell, LTO half-cell, and the LFP//LTO full cell with sputtered metal film CCs at 0.1C. (b) EIS spectra of the LFP//LTO full cells with different CCs. (c) Cycling performance of LFP//LTO full cells with different CCs at 1C.

also exhibited excellent electrochemical cycling stability with 91.6% capacity retention after 400 charge and discharge cycles at 1C (Fig. 4c). Figs. S13a and f displays the cross-sectional SEM images and corresponding EDS mappings of the LFP//LTO cell after cycling. As can be seen, the sputtered CCs are in close contact with the neighboring components. Additionally, the sputtered Al and Cu CCs maintained their dense morphologies after long cycling, suggesting good mechanical strength of CCs (Figs. S13b–e). This result implies the sputtered CCs have good electrochemical stability, accounting for the excellent cycling performance of the AIO lithium-ion battery.

To further demonstrate the compatibility of sputtered current collectors with other electrode systems, traditional lithium-ion battery electrodes LiCoO₂ (LCO), LiNi_{0.8}Co_{0.15}Al_{0.05}O₂ (NCA) and graphite were selected and tested. The LCO/Sputtered Al CC based half-cells exhibited a characteristic discharge voltage plateau at 3.9 V, along with a high capacity retention of 94% after 100 cycles (Fig. 5a and b). This implied that the ultra-thin Al CC is also electrochemically stable at high working voltages. Additionally, in the LCO//LTO full cell system, the AIO cells showed good cycling performance with 89% capacity retention after 400 cycles (Fig. 5c and d). Similarly, the NCA electrode with sputtered CC and NCA//Graphite cell also showed high cycling stability (Figs. S14 and S15 and Fig. 5e). These results demonstrate that the ultrathin sputtered metal films can function as stable current collectors in lithium-ion battery systems.

Owing to the reduced thickness, the ultrathin metal film CCs possess a much lower mass density compared with metal foil CCs (0.46 mg cm⁻², 1.72 mg cm⁻² for Al, Cu metal film, 3.24 mg cm⁻², 8.28 mg cm⁻² for Al foil with 12 μm and Cu foil with 9 μm thickness respectively). Thereby, leveraging the ultrathin metal films instead of traditional metal foils as CCs can reduce the mass proportion of the CCs in the battery, and further increase the overall energy density of the battery. Moreover, for the AIO cells, even at higher mass loadings/areal capacities, the specific capacity of active material LTO is comparable to that of the full-cell with an areal capacity of 1 mAh cm⁻² (Fig. 6a). The mass fraction of primary components in the 1 mAh cm⁻² LFP//LTO full cells are presented as the pie charts (insert in Fig. 6c). Among them, the mass of active materials, binder, and the conductive additive was considered in electrodes when calculating. As shown in the pie charts, comparing to 35% for the mass proportion of CCs in traditional metal foil based cells, the mass proportion of sputtered metal film CCs in the AIO full-cells is only 10%. Based on the mass parameters of 1 mAh cm⁻² full-cell, the mass proportion of two different CCs versus the cell's areal capacities can be calculated and plotted (Fig. 6c). Even at high areal capacity (e.g. 3 mAh cm⁻²), replacing the metal foil with the sputtered metal film as CCs can reduce the mass contribution of CCs by 74% to the battery.

Energy densities of the full cells using metal foil or sputtered metal film as CCs were also calculated and compared (Fig. 6b). When the areal capacity of the full cell was 0.5 mAh cm⁻², the energy density of the

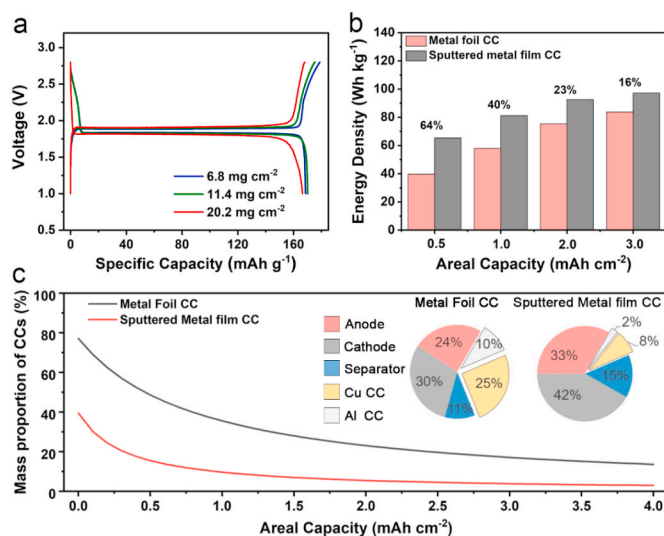


Fig. 6. The mass distribution and energy densities of AIO LFP//LTO full cells based on sputtered metal film CCs and traditional stacked LFP//LTO full cells based on metal foil CCs. (a) GCD profiles of AIO full cells with different mass loadings of LTO at 0.1C. (b) Comparison of energy densities of different full cells, which was calculated based on the total mass of electrodes, separator and CCs. (c) The calculated mass proportion of CCs versus the areal capacity in AIO full cells. The insert pie charts show the mass fraction of the primary components for full cells using different CCs, in which the areal capacity in all cells is fixed at 1 mAh cm⁻².

sputtered metal film CCs based full-cell shows a 64% improvement than that using metal foil CCs. It is worth noting that the improvement of energy density would become more significant when the areal capacity decreases below 0.5 mAh cm⁻². When the cell capacity reaches the commercial level of 3 mAh cm⁻², the achievable energy density improvement is expected to be high as 16%. The above calculations are based on one single cell, and in commercial applications, multiple cells are usually stacked and packaged as soft-packaged batteries. To explore the energy density improvement of the ultra-thin CCs based battery package in practical application, we referred to the parameters of a 52 Ah graphite//NCM soft-packaged battery listed by Wood [5]. Energy densities of batteries using two different kinds of CCs were calculated separately, with the parameters and calculation results listed in Table S3. The calculation result showed that the energy density of battery using the ultra-thin CCs can be increased by 23.7% comparing with that of a traditional battery. Furthermore, our metal film CCs based AIO LIB also exhibits obvious advantages in energy density and cycle performance when compared with recently reported special-shaped LIBs, as

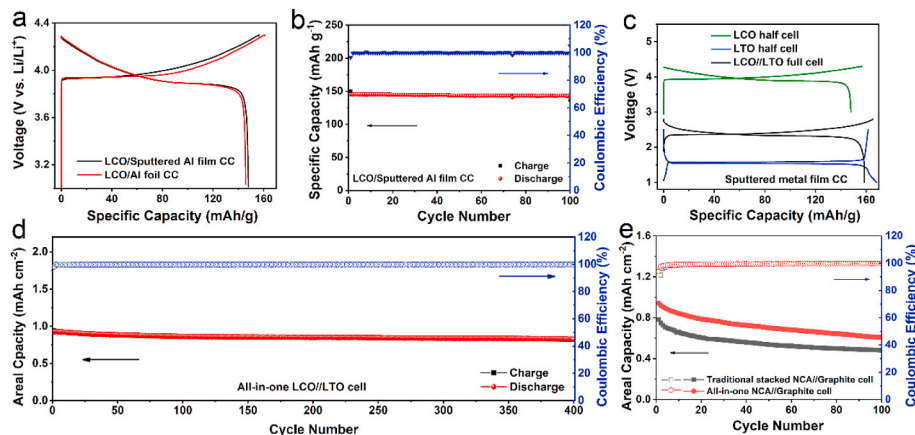


Fig. 5. The compatibility of sputtered metal current collectors with traditional lithium-ion battery electrodes. (a) Galvanostatic charge/discharge profiles at the first cycle of LCO/Sputtered Al CC and LCO/Al foil electrodes half-cell at 0.1C. (b) Cycling performance at 0.5C of LCO//Li half-cell with sputtered Al current collector. (c) The first cycle GCD profiles of LCO half-cell, LTO half-cell, and the LCO//LTO full cell with sputtered metal film CCs at 0.1C. (d) Cycling performance of LCO//LTO AIO full-cell with sputtered CC at 1C. (e) Cycle performance of NCA//Graphite full-cells with different CCs at 1C.

listed in Table S4.

The charge/discharge performance of LIBs sensitively depends on the configuration or geometry of battery [26,27] and further influence the safety characteristic of cells. Therefore, the safety issue that may introduced by this AIO battery configuration change should be concerned. Researches [28,29] have shown that the lithium deposition preferentially occurs at the edges of the anode which could lead to dendrite growth and internal short-circuit if the electrodes cannot overlap completely. Mislocation between cathode and anode may lead to an internal short-circuit. The mislocation fails often occur when the traditional laminated battery is improperly assembled or suffered crashed in the later operation. Therefore, accuracy for positional alignment of the cathode vs. the anode is essential for cell safety. As this paper shows, the all-in-one configuration will improve the adhesion between electrodes and separator. Thus it will help to limit the risk of internal short-circuit. On the other side, the all-in-one battery assembly is a separator-based process that requires the separator to have a high quality including high mechanical strength, few defects, and high electrochemical stability. If the separator can't meet these requirements, it could lead to micro-short circuits during electrode slurry printing, rolling process, or the long term charge/discharge cycling.

To demonstrate the practical applicability and highlight the shape conformability of the ultrathin CCs based battery, we assembled our AIO battery on a flapping wing bird-shaped air vehicle to power its flight. For these air vehicles, flight endurance is one of the key concerns [30]. Equipping micro-aircrafts with conventional battery packs with fixed sizes and shapes (cylindrical or rectangular shape in most cases) can guarantee a high working endurance but will increase the weight and necessitate additional modifications of devices [31]. As a result, the large mass and fixed space requirements of these energy storage components will hinder the various shape design and multi-functional innovations of electronics [32]. Aiming to facilitate the advent of power source-unitized electronics, shape-conformable batteries have become more and more significant [33]. In principle, shape conformable batteries with lightweight feature shall be designed to fit the complex shape of various air vehicles, which can flexibly utilize most of the remaining space of air vehicles to increase the flight endurance without redesigning the vehicle structure. In this respect, the AIO battery technology based on printing and sputtering process is expected to be a promising solution, which can not only realize various shapes especially some complex shapes (see Fig. S16), but also be scaled up with high energy density.

For demonstration, a bird-belly-shaped AIO pouch cell (LCO//LTO) based on ultrathin CCs was designed for the bird-shaped air vehicle (Fig. 7a–c) which was packed into an aluminum-plastic package (Fig. 7d). One battery's capacity is 15 mAh at 0.1C and the voltage platform is 2.4 V (Fig. 7e) which is consistent with the test results of the corresponding coin cells. Additionally, Ni and Al tabs were bonded with the anode and cathode CCs separately by conductive carbon glue for current input and output (see details in the experimental section). As shown in Fig. 7f, two belly-shaped batteries were connected in series and attached tightly to both sides of the bird's belly to power its flight. Because of the shape design, the belly battery can fit the 'bird' body well. The robot bird is only driven by these two batteries and starts flapping its wings when the switch is connected (see Fig. 7g–i and Video S1). The AIO battery has a total geometric area of nearly 20 cm² with a mass of 1.47 g, showing a 9.8% weight reduction and 17% energy density improvement compared with conventional metal foil based battery. If there are more cell layers in one package bag, the improvement of energy density will be more significant (Fig. 7j).

Supplementary video related to this article can be found at <https://doi.org/10.1016/j.jpowsour.2021.229527>

4. Conclusions and outlooks

In summary, we developed a versatile technology for the fabrication of ultrathin CCs based all-in-one LIBs with high gravimetric energy

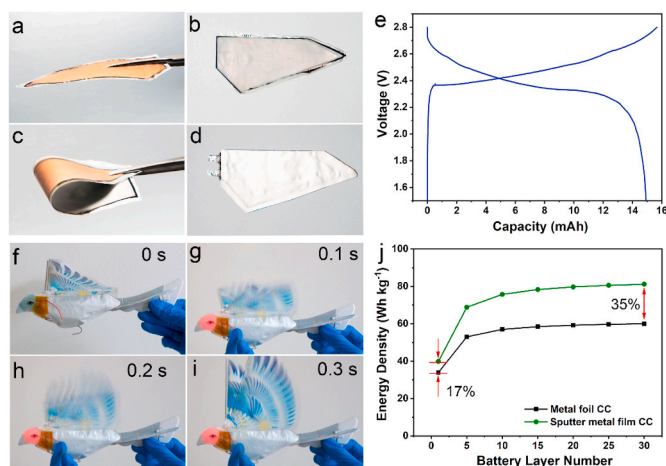


Fig. 7. Demonstration of the shape-conformable (belly-shaped) LCO//LTO battery with sputtered ultrathin CCs. (a–c) Digital photos of the belly-shaped electrodes with ultrathin CCs. (d) Digital photo of the belly-shaped pouch cell. (e) GCD profiles of the AIO belly-shaped pouch cell at 0.1C. (f) Digital photos of the bird-shaped air vehicle connected with two belly-shaped pouch cells. (g–i) Digital photos showing that the bird-shaped air vehicle was powered by two belly-shaped pouch cells. (j) The energy density as a function of battery layer number in one pouch cell based on metal CCs or sputtered ultrathin CCs.

density and shape diversity, via industry-available stencil printing and magnetron sputtering techniques. The layer-by-layer construction technology based on PP separator enables the production of ultrathin metal CCs which can improve the LIB's energy density by 16%–64%. we found it is feasible to magnetron deposit metal film on the active material layer as LIB's CCs. Benefiting from the high electronic conductivity of CCs and high interlayer adhesion of the all-in-one cell, the ultrathin CCs based LIBs (LFP//LTO and LCO//LTO) exhibited outstanding cycling stability (155 mAh g⁻¹ at 1C with over 90% capacity retention after 400 cycles) even at high active mass loading (>7 mg cm⁻²). Besides, owing to the unique stencil printing process in our technology, shape-conformable LIBs can be more easily realized compared with traditional battery technologies. Because of that, this new technology has opened a window for involving thinner CCs in the process of scalable production of LIBs, which can fundamentally solve the high proportion of inactive components issue. For demonstration, bird belly-shaped lithium ion pouch cells were fabricated and seamlessly integrated into a bird-shaped flapping wind vehicle, presenting an enhanced flight time endurance. This solution combines industrially-mature processing technologies that are compatible with current LIBs production chain, holding great potential in the application of smart electronic products with high energy density and shape versatility demands.

Based on this technology, in future work, people may pay attention to further optimize battery electrochemical performance by adopting the following strategies: (1) Develop better tabs connection methods to improve the adhesion and reduce the contact resistance between tabs and electrodes; (2) Adopt stepwise sputtering method for multi-layer metal film CCs to adapt to active material with higher capacity (large volume change) and alleviate the interfacial stress; (3) Involve more efficient packaging methods and lighter packaging materials for high energy special-shaped batteries fabrication. (4) The compatibility of solid-state electrolytes with our sputtering current collector system is also worth further studies. Fabricated following the electrode printing and CC sputtering process, the AIO cell based on solid-state electrolytes shall have better bindings between the electrolyte, electrodes, and current collectors, which is beneficial for the electrochemical performance. For practice application, the cost of magnetron sputtering from energy consumption could be the main concern for adopting this technology in the battery manufacturing industry. It is worth noting that roll-to-roll magnetron sputtering has been widely adopted in industry to prepare

functional films for decades, and thus there is much room for cost reduction for future large-scale manufacturing.

Declaration of competing interest

The authors declare that they have no known competing financial interests or personal relationships that could have appeared to influence the work reported in this paper.

Acknowledgments

The authors thank the Local Innovative and Research Teams Project of Guangdong Pearl River Talents Program (2017BT01N111), Shenzhen Geim Graphene Center, the National Nature Science Foundation of China (Project Nos. 21950410512, 52005289), Guangdong Province Science and Technology Department (Project No. 2020A0505100014), Shenzhen Technical Project (Project No. JCYJ20170412171720306, JSGG20191129110201725) and Tsinghua Shenzhen International Graduate School Overseas Collaboration Project for financial supports.

Appendix A. Supplementary data

Supplementary data to this article can be found online at <https://doi.org/10.1016/j.jpowsour.2021.229527>.

Supplementary data associated with this article can be found in this submission, including SEM spectra, charge/discharge curves, long-life cycling performances, dual-prob resistance, and EIS test of cells.

References

- [1] A. Sumboja, J. Liu, W.G. Zheng, Y. Zong, H. Zhang, Z.J. Liu, Electrochemical energy storage devices for wearable technology: a rationale for materials selection and cell design, *Chem. Soc. Rev.* 47 (2018) 5919–5945.
- [2] J.W. Choi, D.J.N.R.M. Aurbach, Promise and reality of post-lithium-ion batteries with high energy densities, *Nat. Rev. Mater.* 1 (2016) 16013–16028.
- [3] Y. Liang, C.Z. Zhao, H. Yuan, Y. Chen, W. Zhang, J.Q. Huang, A review of rechargeable batteries for portable electronic devices, *Info 1* (2019) 6–32.
- [4] B.A. Johnson, R.E. White, Characterization of commercially available lithium-ion batteries, *J. Power Sources* 70 (1998) 48–54.
- [5] D.L. Wood III, J. Li, C. Daniel, Prospects for reducing the processing cost of lithium ion batteries, *J. Power Sources* 275 (2015) 234–242.
- [6] W. Pflöging, A review of laser electrode processing for development and manufacturing of lithium-ion batteries, *Nanophotonics* 7 (2018) 549–573.
- [7] H. Cheskis, S. Chen, W. Brenneman, T. Ozaki, Ultra thin copper foil for HDI applications, *Circuitree Campbell* 17 (2004) 10–19.
- [8] H. Cheskis, W. Brenneman, S. Chen, Copper Foil for HDI Applications, 2001 IPC Expo Proceedings, 2001.
- [9] D. Andre, S.J. Kim, P. Lamp, S.F. Lux, F. Maglia, O. Paschos, Future generations of cathode materials: an automotive industry perspective, *J. Mater. Chem.* 3 (2015) 6709–6732.
- [10] W.J.N. Pflöging, A review of laser electrode processing for development and manufacturing of lithium-ion batteries, *Nanophotonics* 7 (2018) 549–573.
- [11] K.Y. Kang, Y.G. Lee, D.O. Shin, J.C. Kim, K.M. Kim, Performance improvements of pouch-type flexible thin-film lithium-ion batteries by modifying sequential screen-printing process, *Electrochim. Acta* 138 (2014) 294–301.
- [12] J.H. Yun, G.B. Han, Y.M. Lee, Y.G. Lee, K.M. Kim, J.K. Park, Low resistance flexible current collector for lithium secondary battery, *Electrochem. Solid State Lett.* 14 (2011) 116–119.
- [13] K. Wang, X. Zhang, C. Li, X. Sun, Q. Meng, Y. Ma, Chemically crosslinked hydrogel film leads to integrated flexible supercapacitors with superior performance, *Adv. Mater.* 27 (2015) 7451–7457.
- [14] M. Koo, K.I. Park, S.H. Lee, M. Suh, D.Y. Jeon, J.W. Choi, Bendable inorganic thin-film battery for fully flexible electronic systems, *Nano Lett.* 12 (2012) 4810–4816.
- [15] Y. Wang, S. Su, L. Cai, B. Qiu, N. Wang, J. Xiong, Monolithic integration of all-in-one supercapacitor for 3D electronics, *Adv. Energy Mater.* 9 (2019) 1900037.
- [16] A. Liu, P. Kovacic, N. Peard, W. Tian, H. Goktas, J. Lau, Monolithic flexible supercapacitors integrated into single sheets of paper and membrane via vapor printing, *Adv. Mater.* 29 (2017) 1606091.
- [17] C. Jiang, Y. Fang, J. Lang, Y. Tang, Integrated configuration design for ultrafast rechargeable dual-ion battery, *Adv. Energy Mater.* 7 (2017) 1700913.
- [18] N. Wang, G. Han, Y. Xiao, Y. Li, H. Song, Y. Zhang, Polypyrrole/graphene oxide deposited on two metalized surfaces of porous polypropylene films as all-in-one flexible supercapacitors, *Electrochim. Acta* 270 (2018) 490–500.
- [19] M. Haruta, S. Shiraki, T. Suzuki, A. Kumatani, T. Ohsawa, Y. Takagi, Negligible “negative space-charge layer effects” at oxide-electrolyte/electrode interfaces of thin-film batteries, *Nano Lett.* 15 (2015) 1498–1502.
- [20] C. Liu, E.I. Gillette, X. Chen, A.J. Pearce, A.C. Kozen, M.A. Schroeder, An all-in-one nanopore battery array, *Nat. Nanotechnol.* 9 (2014) 1031.
- [21] S. Ferrari, M. Loveridge, S.D. Beattie, M. Jahn, R.J. Dashwood, R. Bhagat, Latest advances in the manufacturing of 3D rechargeable lithium microbatteries, *J. Power Sources* 286 (2015) 25–46.
- [22] M. Yao, R. Wang, Z. Zhao, Y. Liu, Z. Niu, J. Chen, A flexible all-in-one lithium-sulfur battery, *ACS Nano* 12 (2018) 12503–12511.
- [23] C.T. Love, Thermomechanical analysis and durability of commercial micro-porous polymer Li-ion battery separators, *J. Power Sources* 196 (2011) 2905–2912.
- [24] R.F. Messier, The nano-world of thin films, *J. Nanophotonics* 2 (2008), 021995.
- [25] J. Huang, Z. Qi, L. Li, H. Wang, S. Xue, B. Zhang, Self-assembled vertically aligned Ni nanopillars in CeO₂ with anisotropic magnetic and transport properties for energy applications, *Nanoscale* 10 (2018) 17182–17188.
- [26] B. Son, M.-H. Ryou, J. Choi, S.-H. Kim, J.M. Ko, Y.M. Lee, Effect of cathode/anode area ratio on electrochemical performance of lithium-ion batteries, *J. Power Sources* 243 (2013) 641–647.
- [27] P.J. Osswald, S.V. Erhard, J. Wilhelm, H.E. Hoster, A. Jossen, Simulation and measurement of local potentials of modified commercial cylindrical cells, *J. Electrochem. Soc.* 162 (2015) A2099–A2105.
- [28] M. Tang, P. Albertus, J. Newman, Two-dimensional modeling of lithium deposition during cell charging, *J. Electrochem. Soc.* 156 (2009) A390.
- [29] T. Dagger, J. Kasnatscheew, B. Vortmann-Westhoven, T. Schwieters, S. Nowak, M. Winter, et al., Performance tuning of lithium ion battery cells with area-oversized graphite based negative electrodes, *J. Power Sources* 396 (2018) 519–526.
- [30] A. Perez-Rosado, R.D. Gehlhar, S. Nolen, S.K. Gupta, H.A. Bruck, Design, fabrication, and characterization of multifunctional wings to harvest solar energy in flapping wing air vehicles, *Smart Mater. Struct.* 24 (2015), 065042.
- [31] C.A. Aubin, S. Choudhury, R. Jerch, L.A. Archer, J.H. Pikul, R.F. Shepherd, Electrolytic vascular systems for energy-dense robots, *Nature* 571 (2019) 51–57.
- [32] K.H. Choi, D.B. Ahn, S.Y. Lee, Current status and challenges in printed batteries: toward form factor-free, monolithic integrated power sources, *ACS Energy Lett* 3 (2017) 220–236.
- [33] S.H. Kim, K.H. Choi, S.J. Cho, S. Choi, S. Park, S.Y. Lee, Printable solid-state lithium-ion batteries: a new route toward shape-conformable power sources with aesthetic versatility for flexible electronics, *Nano Lett.* 15 (2015) 5168–5177.